KSME

Springer

Journal of Mechanical Science and Technology 36 (1) 2022

Original Article
DOI 10.1007/s12206-021-1214-8

Keywords:
· Hydrogen embrittlement
· 316L stainless steel
· Slow strain rate tensile test
· Fatigue life
· Low temperature

Correspondence to:
Un Bong Baek
ubbaek@kriss.re.kr

Citation:
Nguyen, T. T., Park, J., Nahm, S. H., Baek, U. B. (2022). An experimental study for qualifying hydrogen compatibility of austenitic stainless steel under low temperature. Journal of Mechanical Science and Technology 36 (1) (2022) 157~165. http://doi.org/10.1007/s12206-021-1214-8

Received May 16th, 2021
Revised August 5th, 2021
Accepted September 24th, 2021

† Recommended by Editor Chongdu Cho

An experimental study for qualifying hydrogen compatibility of austenitic stainless steel under low temperature

Thanh Tuan Nguyen, Jaeyeong Park, Seung Hoon Nahm and Un Bong Baek

Team of Hydrogen Energy Materials Research, Korea Research Institute of Standard and Science, 267 Gajeong-Ro, Yeseong-Gu, Daejeon 34113, Korea

Abstract Hydrogen compatibility of materials refers to the ability to exhibit reliable mechanical integrity and a probability of failure in a given hydrogen-exposed environment. Currently, no experimental methods for qualifying the hydrogen compatibility of materials have been standardized, and testing expertise has been restricted to only a few laboratories. With international coordination, this paper presents the experimental activities and results to establish a code of practice. The experimental campaign included a slow strain rate tensile (SSRT) test and a notched fatigue life test on SUS316L-grade austenitic stainless steel, which has been widely used in structural components in hydrogen service. Sub-sized tensile specimens were machined from a bar with a gauge diameter of 4.00 mm and a gauge length of 20 mm. A notched specimen with a notch angle of 60°, notch radius of 0.12 mm, and net section diameter of 4 mm was prepared for the fatigue life test. The net section stress in the notched specimen at maximum load (σ_{max}) was 444 MPa in a tension–tension loading condition with a loading ratio of R = 0.1. The tests were performed at a temperature of 233 K (-40 °C) in two environmental conditions: high-pressure hydrogen gas at 90 MPa and nitrogen gas at 0.1 MPa (three tests for each condition). No noticeable degradation in yield strength and tensile strength was observed in the specimens tested under hydrogen pressure of 90 MPa H_2 at -40 °C compared to that tested 0.1 MPa N_2 at -40 °C, however, hydrogen had a remarkable effect on reduction area (RA), and strain at fracture. The consistency of the experimental conditions and results from different laboratories with a distinct testing system were closely compared and discussed.

1. Introduction

The infrastructure for onboard storage and transportation of hydrogen is still the main obstacle in accelerating the commercialization of fuel cell vehicles. The design criteria for hydrogen-exposed structures are stricter in terms of material compatibility because hydrogen can degrade the mechanical properties of almost all structural materials [1, 2]. Hydrogen-exposed service components must be designed with a higher safety factor, which is often based on mechanical load, environmental conditions, material performance, and design service life. A performance database and general materials qualification is required for designing components used in hydrogen service. A general method for studying the hydrogen compatibility of materials is a comparison of the mechanical properties of hydrogen-exposed specimens with those of specimens not exposed to hydrogen [3-5]. Testing of hydrogen embrittlement (HE) susceptibility can be based on various testing techniques such as slow strain tensile test (SSRT), S-N fatigue, and fracture mechanics. At present, two methods used to introduce hydrogen into the test sample include: using a pre-charged process (such as electro-chemical charging, thermal charging), or directly exposing in a high-pressure hydrogen environment (in situ testing). Although the HE mechanism may be similar for both test methods, the initial boundary conditions are very different, mostly relating to the difference in the hydrogen distribution on the specimen

Table 1. Chemical composition of SUS316L (wt.%).

C	Si	Mn	P	S	Ni	Cr	Mo
0.019	0.49	1.41	0.029	0.024	12.19	17.13	2.05

[6, 7]. In general, conducting with hydrogen pre-charged specimens required less complicated testing systems compared to the testing method in a gaseous hydrogen environment. In situ testing method may be more appropriate for representing the conditions that components exposed directly to hydrogen gas such as hydrogen vessels, structural pipelines.

The mechanisms of hydrogen-degraded mechanical properties have been extensively investigated in the Refs. [1-3, 5-12]. The group of ferritic/martensitic steels is the most commonly used materials for structural components since these steels often exhibit high strength and toughness at low costs. However, due to low hydrogen solubility and high diffusivity, nearly all body-centered cubic steels exhibit severe susceptibility to HE [13-16]. With the ongoing demand for structural materials for use in the hydrogen economy infrastructure, grade 300 austenitic stainless steel is promising [5-7, 9, 11, 17-19]. It is noted that the HE of austenitic stainless steel is a temperature-dependent and pressure-dependent process. Thus, accurate control of environmental factors is critical in evaluating the hydrogen compatibility of materials. The allowable temperature ranges for the commercial hydrogen storage vessel are from -50 °C to 85 °C. These temperature ranges are generally represented for the extreme ambient temperature conditions to which hydrogen service may expose during actual operating conditions. For example, the onboard hydrogen vessel in the fuel cell vehicle is often cooled to -40 °C before re-fueling. Thus, to build a model that best reflects the operating conditions of the hydrogen vessel, mechanical tests resembling environmental conditions are conducted which are at high-pressure hydrogen and a low-temperature condition. At present, experimental research of its tensile and fatigue life properties in low-temperature and extremely high-pressure gaseous hydrogen environments is limited owing to the complexity of the installation of experimental equipment [11, 17-19]. The main purpose of this research is to provide additional SSRT and notched fatigue life test results for SUS316L austenitic stainless steel in low-temperature and high-pressure hydrogen environments to establish a code of practice. The detailed temperature control and hydrogen gas purity conditions are explained. A comparative analysis of the results obtained under different research institutes may provide an insight into the sensitivity of the hydrogen compatibility of materials to important parameters such as specimen surface and experimental conditions.

2. Experimental setup

2.1 Materials and specimen

Slow strain rate tensile (SSRT) tests and notched fatigue life tests were performed on SUS316L grade austenitic stainless steel. The material composition is presented in Table 1. The reference tensile properties are presented in Table 2. Sub-sized tensile specimens were machined from a bar with a gauge diameter of 4.0 mm and a gauge length of 20 mm in accordance with ASTM E8/E8M [4]. A constant crosshead speed of 10^{-3} mm/s was used in the SSRT test. To avoid potential cracks at the contract point between a contact-type extensometer and the specimen, the extensometer was specifically not used. After the SSRT test, the strain at fracture was evaluated from two marking points on the gauge length of the broken specimens. A notched specimen with a notch angle of 60°, a notch radius of 0.12 mm, and a net section diameter of 4.0 mm were prepared for the notched fatigue life test. Tension–tension notched fatigue life tests were conducted at a stress ratio of R = 0.1 and a test frequency of 1 Hz. The fatigue life tests with the notched specimen were carried out at the maximum load (σ_{max}) was 444 MPa in a tension–tension loading condition with a loading ratio of R = 0.1. The stress value of 444 MPa is corresponding to the net-section stress of 2/3 the measured tensile strength, which is approximately equal to the maximum allowable stress value of this material. The specimen shapes and dimensions are shown in Fig. 1. Surface roughness was measured by a roughness detector (Mitutoyo SJ-410; Mitutoyo Cooperation) with a measuring speed of 0.5 mm/s and cut-off length, λ_c = 0.5 mm.

Table 2. Mechanical properties of the reference material at room temperature.

$\sigma_{0.2}$ [MPa]	σ_{UTS} [MPa]	Elongation [%]	RA [%]
245	551	60	78

Table 3. Conditions of SSRT and notched fatigue tests.

Test	Environment	Conditions	Number of tests
SSRT -40 °C	0.1 MPa N_2	0.001 mm/s	1
	10 MPa N_2	0.001 mm/s	2
	90 MPa H_2	0.001 mm/s	3
Notched fatigue R = 0.1, -40 °C	0.1 MPa N_2	f = 1 Hz, σ_a = 200 MPa	3
	90 MPa H_2	f = 1 Hz, σ_a = 200 MPa	3

2.2 Temperature control

The gaseous hydrogen test system in ambient air was modified to create a low-temperature environment, as shown in Fig. 2. The original equipment was a vessel with a maximum pressure of 120 MPa integrated on a servo-hydraulic material testing frame. The test pressure in the vessel was accurately controlled by a computer in the safety control room. The load generated during the mechanical test process was measured from a load cell inside the autoclave with a maximum capacity

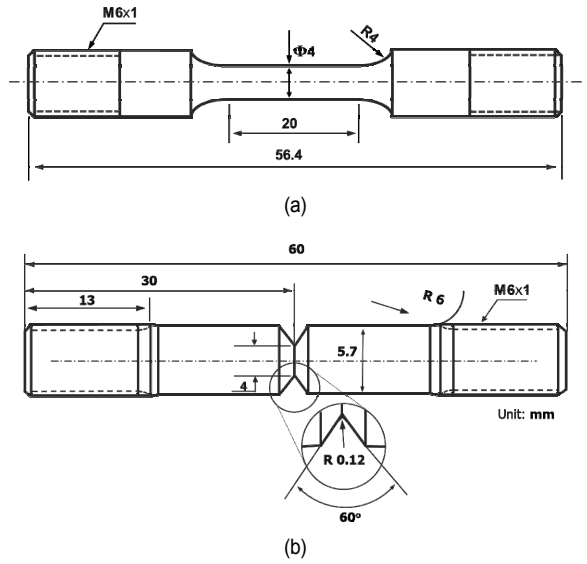

Fig. 1. Schematics of tested specimens: (a) SSRT test specimen; (b) notched fatigue life test specimen.

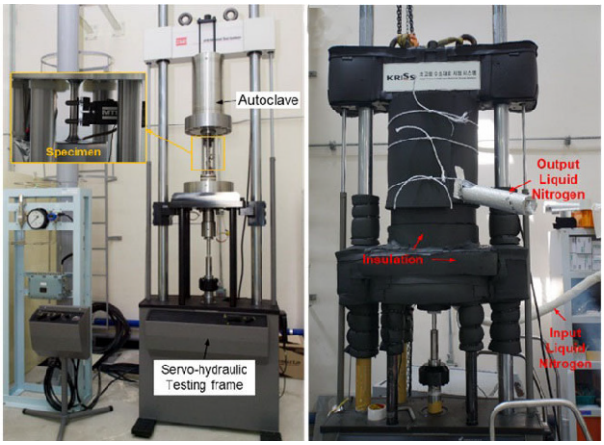

Fig. 2. Experimental setup for testing in (a) the gaseous hydrogen test system in ambient air; (b) gaseous hydrogen test system at low-temperature conditions.

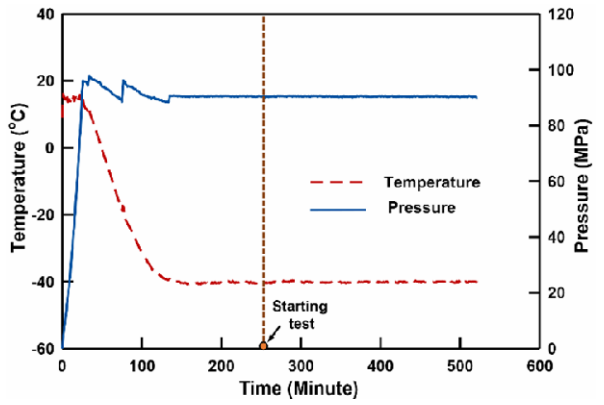

Fig. 3. Variation in temperature and pressure with time from the beginning of cooling to end of the tests.

Table 4. Composition of reference gas for calibration.

O_2+Ar	N_2	CH_4	CO	CO_2	He
5.62	4.57	5.05	5.18	5.53	Bal.

Table 5. Gaseous hydrogen analysis results.

	H_2	CO_2+ CO	N_2	O_2+Ar	CH_4	H_2O
Current study (ppm)	Bal.	0	0.17	0.17	0	0.077
CHCM 1 (ppm)	99.999	2	2	1	1	3.5

of 50 kN; the strains were measured using an extensometer with a gauge length of 25.4 mm inside the pressure vessel. Low-temperature test conditions were produced using a conduction-cooling method to decrease the temperature in the autoclave. To achieve the desired test temperature, the low-temperature flow from the liquid nitrogen tank was injected into a cooling pipe system installed around the autoclave (Fig. 2(b)). The temperature was monitored by thermocouples installed inside the autoclave and on the test specimen. The variation in temperature and pressure with time during the test process is shown in Fig. 3.

2.3 Gas environment preparation

Previous studies have reported that hydrogen gas purity plays a key role in the hydrogen environmental embrittlement (HEE) susceptibility of materials. A small impurity in the hydrogen gas such as carbon monoxide (CO) or oxygen (O_2) can greatly affect the hydrogen-metal surface interaction and reduce the HEE susceptibility [20-23]. Analysis of impurities in the hydrogen gas before testing is necessary to obtain reliable results. The preparation of the gas environment is also important to ensure gas purity. After equipment assembly, the hydrogen environments in the autoclave were carefully produced through vacuuming, and high-purity nitrogen and high-purity helium gas purging. The autoclave was purged with high-purity nitrogen gas (four times) followed by high-purity helium (three times) to 10 MPa. The nitrogen and helium purities were 99.9999 %. Prior to filling with H_2 at the test pressure of 90 MPa, the system was purged three times with high-purity hydrogen gas (99.9999 %). The O_2 content was evaluated using a gas analyzer (DF 370 E), and the presence of H_2O was measured using a moisture analyzer (HALO 3) installed downstream of the testing system. Gas analysis was conducted immediately before the test. The gas analyzer results indicated that the hydrogen gas contained 0.17 ppm O_2, 0.17 ppm N_2, and 0.077 ppm H_2O. The calibration gas used in gas analyzers is also important in the precise evaluation of gas impurities. In our system, gaseous components including O_2, Ar, N_2, CH_4, CO, CO_2, and He was used as the calibration gas. The compositions of the reference gas and the hydrogen gas impurity are presented in Tables 4 and 5, respectively.

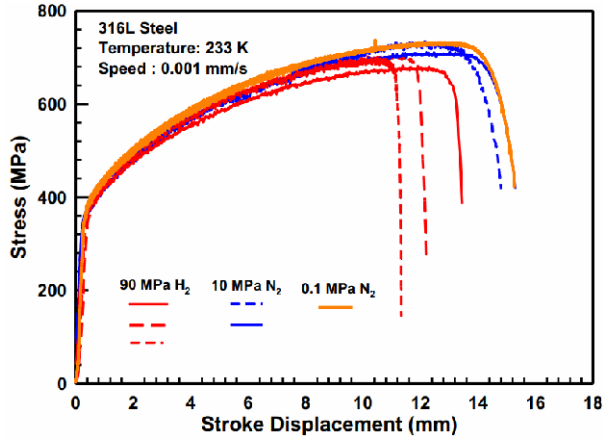

Fig. 4. Nominal stress–stroke displacement curves for SSRT test under different environmental conditions.

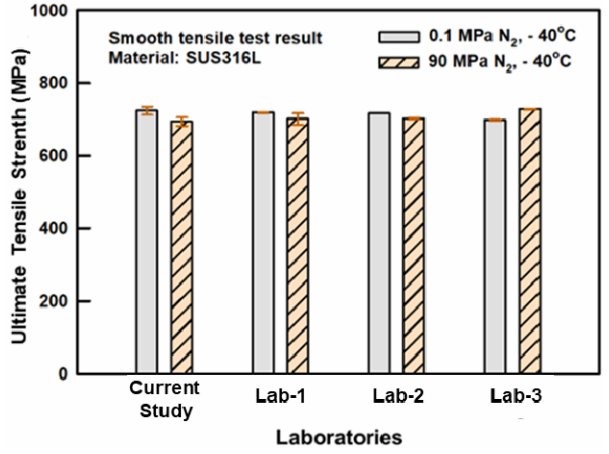

Fig. 5. Comparison of tensile strength in 0.1 MPa N_2 at -40 °C and 90 MPa H_2 at -40 °C among the four research laboratories.

3. Results and discussion

3.1 SSRT test results

Fig. 4 presents a comparison of the nominal stress–stroke displacement curves of SSRT tests for specimens tested in nitrogen and hydrogen gas conditions. The curves nearly coincide from the beginning to the point near the ultimate tensile strength. A clear distinction is only observed near the ultimate tensile strength point. The ultimate tensile strength of the specimen was slightly greater in N_2 gas than in a high-pressure H_2 environment. The ultimate tensile strength values from the four laboratories were comparable, as shown in Fig. 5.

The experimental results for the strength and ductility (elongation and reduction in area) parameters are presented in Table 6. The results from other laboratories; named as Lab-1, Lab-2, Lab-3 are included for comparison [24]. The average strain at fracture was at least 67.9±2.24 % in the N_2 environment while it was approximately 54.0±7 % in 90 MPa H_2, 18.6 % less than in N_2. The RAs are consistent at approximately 81.0 % in the nitrogen-exposed specimens, and approximately 51.0±3 % in 90 MPa-exposed specimens. The variation in the RA presents a trend similar to that of the strain at fracture; however, the RA rate is greater than the strain rate.

Table 6. Summary of SSRT test results under different environmental conditions.

Test cond.	Inst.		Tensile strength (MPa)	EL (%)	RA (%)
0.1 MPa N_2 40 °C	Current study	1*	730	65.3	80.2
		2*	711	69.4	81.7
		3	730	68.9	81.3
		Aver.	721±13	67.4±2.9	81.0±1.1
	Lab-1	Aver.	718	77	83
	Lab-2	Aver.	716	85	84
	Lab-3**	Aver.	698	86.3	84.19
90 MPa H_2 - 40 °C	Current study	1	702	55.5	50.2
		2	698	46.4	49.1
		3	680	61.2	54.4
		Aver.	693±12	54.0±7	51.0±3
	Lab-1	Aver.	701	78	77
	Lab-2	Aver.	702	83	67
	Lab-3	Aver.	728	81.4	61.65

* N_2 pressure: 10 MPa, ** N_2 pressure: 6.5 MPa

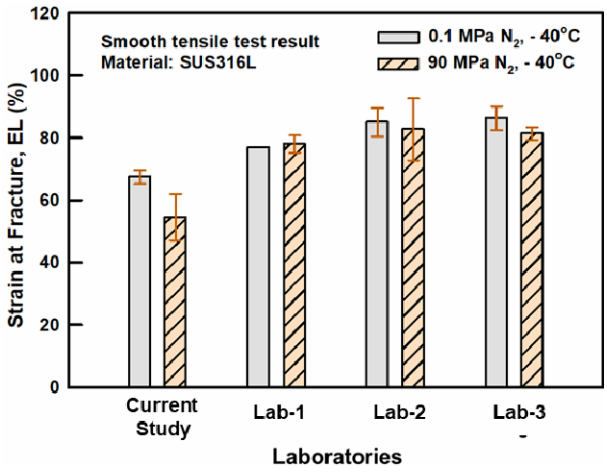

Fig. 6. Comparison of strain at fracture in 0.1 MPa N_2 at -40 °C and 90 MPa H_2 at -40 °C among the four research laboratories.

A comparison of strain at fracture, RA, and relative reduction in area, RAA (RAA = RA_{H2}/RA_{He}) obtained by four laboratories is shown in Figs. 6 and 7. The strain at fracture in the present dataset in an N_2 or H_2 environment was significantly lower than the results from other laboratories. The measured RA of the nitrogen-exposed specimens was consistent among the laboratories; however, there were notable discrepancies in the RA of hydrogen-exposed specimens. As shown in Fig. 7(a), the lowest RA was obtained by the current results, approximately 51 %; the greatest average result was obtained by Lab, approximately 77 %.

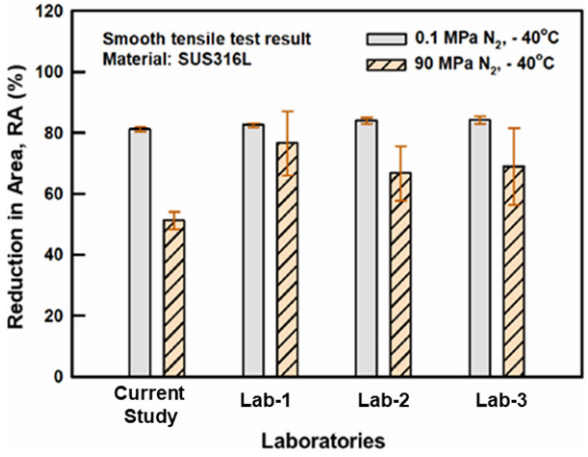

(a)

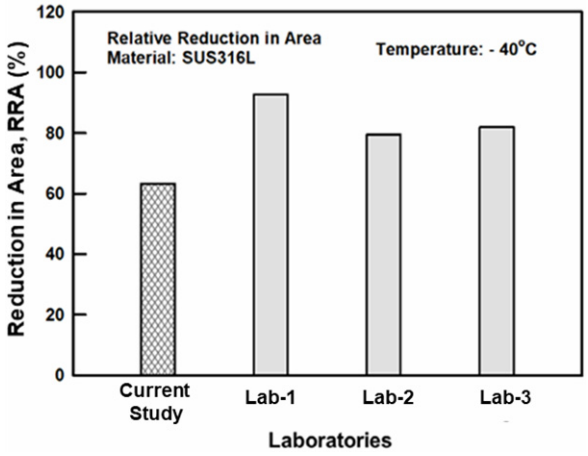

(b)

Fig. 7. Comparison of (a) reduction in area (RA) in 0.1 MPa N_2 at -40 °C and 90 MPa H_2 at -40 °C; (b) relative reduction in area (RAA) among the four research laboratories.

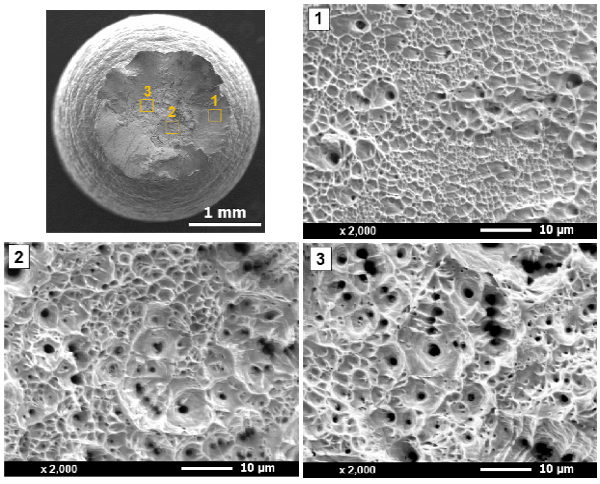

(a)

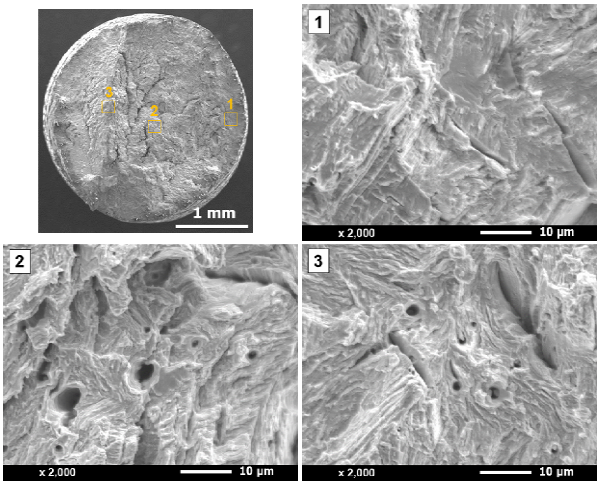

(b)

Fig. 8. Fracture morphology of SSRT specimen in different environmental conditions exhibited significantly different fracture features: (a) 10 MPa N_2 at -40 °C; (b) 90 MPa H_2 at -40 °C.

The values obtained by Lab-2 and Lab-3 were approximately 67 % and 61.65 %, respectively. The variation in the RRA between the four research institutes was similar to the variation in the RA tested in H_2, as shown in Fig. 7(b).

Fig. 8 shows macroscopic and microscopic images comparing the fracture surface in nitrogen and hydrogen gas. In Fig. 8(a), a typical cup-cone fracture can be observed in the nitrogen-exposed specimen, which includes the shear stress fracture region (Fig. 8(a1)) and the purely normal region (Figs. 8(a2) and (a3)). The 90 MPa hydrogen-exposed specimens exhibited significantly different fracture features. The fracture surface was mixed with brittle quasi-cleavage fractures. The outer specimen surface exhibited a predominant brittle intergranular fracture; the inner portion of the fracture surface had a mixture of quasi-cleavage fractures, intergranular fractures, and fine dimples with quasi-cleavage as the dominant fracture mode. The change in the fracture mechanism with the distance from the outer surface is attributed to the difference in hydrogen. It is well-established that locations with a high defect density in the metal lattice such as austenite grain boundaries are often preferential for hydrogen trap sites. The early critical hydrogen content for hydrogen-assisted crack initiation near the surface may lead to the formation of crack initiation sites along the austenite grain boundary, resulting in a dominant intergranular fracture, as shown in Fig. 8(b1). At a certain crack path propagation in the inner portion, some active fracture mechanisms are completed, such as the formation of microvoids and crack propagation, resulting in a mixture of dimple, intergranular, and quasi-cleavage fractures, as shown in Figs. 8(b2) and (b3).

3.2 Fatigue test results

Fig. 9 shows a comparison of the fatigue life on the notched specimen in 0.1 MPa N_2 and 90 MPa H_2. The results obtained by other research institutes are included for comparison. The average fatigue life of specimens in 0.1 MPa N_2 at -40 °C is approximately 20655 cycles. The average fatigue life in

Table 7. Notched fatigue life test results.

Laboratory		0.1 MPa N_2 -40 °C	90 MPa H_2 -40 °C
Current study	1	21645	9327
	2	22455	11081
	3*	17866	11921
	Aver.	20655±2449	10776±1323
Lab-1	Aver.	21829	11558
Lab-2	Aver.	24033	9983

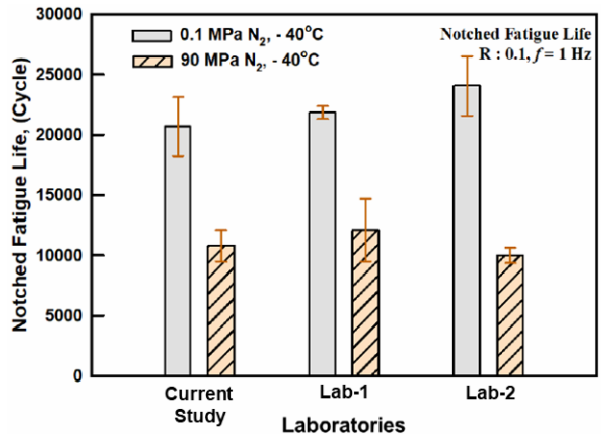

Fig. 9. Comparison of average fatigue life in 0.1 MPa N_2 at -40 °C and 90 MPa H_2 at 40 °C among the three laboratories.

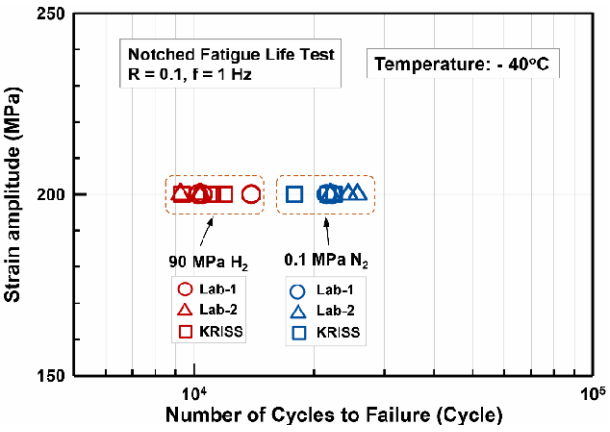

Fig. 10. Comparison of nominal stress amplitude versus number of cycles to failure diagram among datasets obtained from KRISS, Lab-1 and Lab-2.

90 MPa H_2 at -40 °C is approximately 10776 cycles, approximately 50 % less than in an N_2 environment, as shown in Table 7. The fatigue life results are comparable among the three laboratories, in both 0.1 MPa N_2 and 90 MPa H_2 environments. Fig. 10 presents a comparison of the nominal stress amplitude-fatigue life diagrams for the laboratories. The square symbols indicate the current results; the open triangles and open circles indicate the results reported by Lab-1 and Lab-2, respectively. Although the fatigue life was not always the same at different laboratories, the fatigue life range and average

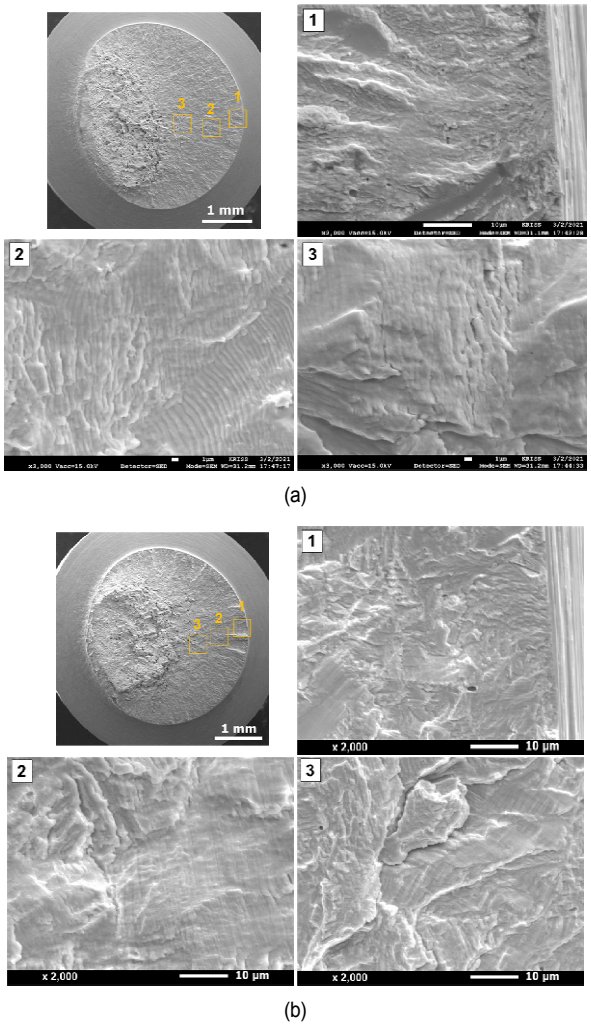

Fig. 11. Macroscopic and microscopic images of fracture surfaces after fatigue life test: (a) nitrogen-exposed specimen; (b) hydrogen-exposed specimen.

were comparable among the three laboratories.

Fig. 11 shows typical macroscopic and microscopic images of the fracture surfaces observed by SEM after the fatigue life test for both nitrogen-exposed and hydrogen-exposed specimens. In the macroscopic observation, all fracture surfaces presented similar features with two distinct regions: fatigue fracture and overload fracture regions. Detailed microscopic observations were performed at several locations from the crack initiation site to the region near the overload fracture area. The crack initiation sites in both specimens were completely flat and decorated with facets. Striation forms were clearly observed on the fracture surface of the nitrogen-exposed specimen, representing a typical fracture mechanism in the fatigue failure of ductile materials, as shown in Fig. 11(a). The microfracture surface of the hydrogen-exposed specimen was decorated with a mixture of quasi-cleavage fracture and striation marks (Fig. 11(b)). Striation patterns were observed, but the fraction area where striation forms appeared was less distinct than in the nitrogen-exposed specimen.

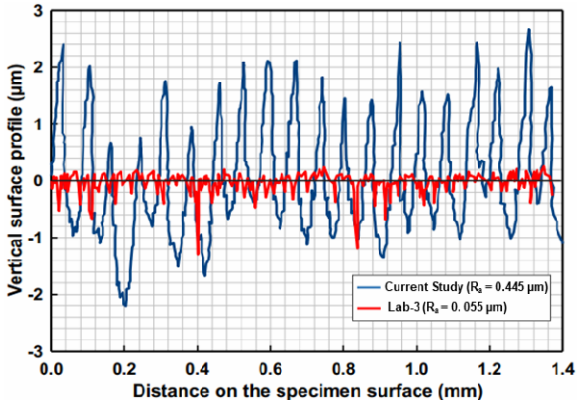

Fig. 12. Comparison of the initial surface roughness profile between the current and Lab-3's specimen.

3.3 Discussion

The effect of high-pressure hydrogen and temperature on the mechanical properties of group 300 austenitic stainless steel has been extensively researched [1-3, 5, 6, 10-12]. The yield strength was not affected by gaseous hydrogen; the ultimate tensile strength was slightly decreased. It is attributed to the austenitic stainless steel with a high nickel content (N_{ieq} = 28.01) can retain its stability under a uniform deformation process regardless of hydrogen conditions [5]. Irrespective of the experimental conditions in different laboratories, the ultimate tensile strength results were comparable in nitrogen and hydrogen environments. Quantitative values related to ductility properties such as the RAs and RRAs have been widely used as material selection criteria for structural components in hydrogen service. In Fig. 6(a), there is no significant difference in the RA of the nitrogen-exposed specimen among the four laboratories. However, there are notable discrepancies in the strain at fracture, RA, and RAA in datasets obtained from the different laboratories, meanwhile the results in the current study in 90 MPa H_2 at 40 °C were the lowest. Because the test material was from the same supplier, the discrepancies in the results can be attributed to differences in the experimental preparation for testing the hydrogen environment or the specimen conditions. Preparation of the hydrogen test environment is important for the precise evaluation of gas impurities. From the literature review, impurities in a hydrogen gas environment may have inhibitory effects on the hydrogen-induced degradation of tensile and fatigue properties. Oxygen is an impurity most likely to be present in H_2 test environments. Precise evaluation of the oxygen content is critically important to accurately evaluate the hydrogen compatibility of materials [20-23]. As shown in Table 6, the impurity analysis results in H_2 testing exceeded the CHCM-1 standard requirement [24]. Although there is no specific gas impurity analysis data from other institutes, it is clear that the hydrogen gas purity was strictly controlled. However, it is important to note that the oxygen concentration contained in hydrogen can be gradually increased with exposure time when hydrogen is stored in a closed vessel [21]. This factor can also show an inhibitory effect on the HEE susceptibility of materials.

In the aforementioned discussions, H_2 gas impurities might be excluded as a primary reason for the discrepancy. In discussions with the other institutes, the difference in the experimental sample conditions became apparent, not only the surface roughness but also residual stress and work hardening in the material layer near the outer surface. It has been reported that surface roughness plays important role in the interaction between hydrogen and metal surface. Ez-Zaki et al. reported that the susceptibility to HE increases significantly with the increase of the surface roughness from R_a = 0.03 μm to 0.5 μm [22, 25]. Prior to the experiment in a hydrogen gas environment, the specimen surfaces in Lab-1, Lab-2, and Lab-3 [26] were carefully finished by mechanical polishing and buffing. However, the present experiments did not include mechanical grinding and polishing. Fig. 12 presents a comparison of the typical roughness profile between the current and Lab-3's specimens. The surface roughness, R_a of the present specimen was about 0.445 μm while the estimated value on Lab-3's specimen is only about 0.055 μm which is approximately 10 times lower than that in the current specimen. Therefore, irregularities left during the machining process can become sites of stress concentration, which can increase both hydrogen trapping and the rate of hydrogen diffusion, and act as preferred sites for hydrogen-assisted crack initiation, resulting in a reduced strain at fracture, RAs, and RAAs. The implementation of research to clarity a synergistic effect of the specimen surface conditions, and gas purity on the SSRT test results, will be investigated in future work.

The differences in the notched fatigue life in the hydrogen-exposed specimen datasets are not distinct compared to those of the strain at fracture, RA, or RAAs. Scatters in the fatigue life in both nitrogen and hydrogen environments are often expected, especially in a low-stress amplitude regime, mainly attributed to the anomalous initiation and propagation of small fatigue cracks at the notched location. As above-mentioned results, the main reason for the difference between the present results for SSRT under 90 MPa H_2 and those of other research institutes is the difference in the state of the experimental specimen surface. A pre-existing scratch-like notch can strongly affect the specimen surface reaction to hydrogen. However, the notched fatigue specimen was tested to mitigate the formation of a large plastic strain in the gauge length. The high stress/strain localization at the notch root can also increase the rate of hydrogen diffusion and the number of hydrogen traps on a larger scale. Thus, less distinct differences in the fatigue life among the four laboratories can be attributed to the effect of the stress triaxiality on hydrogen diffusion, which dominated the effect of the specimen surface conditions.

4. Conclusions

SSRT and notched fatigue life tests of SUS316L austenitic stainless steel were performed in high-pressure hydrogen and

nitrogen gas at -40 °C. The test results were compared with those of other research laboratories to clarify the effect of the experimental conditions. The following conclusions were drawn:

1) No remarkable degradation in the ultimate tensile strength was observed in the specimens tested under high-pressure hydrogen of 90 MPa H_2 at -40 °C, compared to that tested 0.1 MPa N_2 at -40 °C. 90 MPa H_2 at -40 °C had a significant effect on RA and strain at fracture.

2) The estimated tensile strengths were comparable to those obtained by other laboratories, however, there were remarkable discrepancies in the strain at fracture, RA in the hydrogen-exposed specimens. The differences in the hydrogen compatibility of materials are attributed mainly to the differences in the experimental specimen, and environmental conditions.

3) The fatigue life of the specimen exposed to 90 MPa H_2 at -40 °C is approximately reduced by 50 % compared to that tested in N_2 environment. The less distinct differences in the fatigue life among the three laboratories can be attributed to the effect of the stress triaxiality on hydrogen diffusion. The high stress/strain localization at the notch root can enhanced hydrogen diffusion rate and hydrogen traps which dominated the specimen surface conditions dependency of hydrogen-assisted fracture.

Acknowledgments

This work was supported by the 2019~2021 KAIA/MOLIT Project (No.19TLRP-C152334-01) leaded by Korea Research Institute of Standards and Science (KRISS), Republic of Korea.

Nomenclature

EL : Elongation, %
HEE : Hydrogen environment embrittlement
R : Loading ratio
RA : Reduction in area, %
RRA : Relative reduction in area
SSRT : Slow strain rate tensile
σ_a : Nominal stress amplitude, MPa
$\sigma_{0.2}$: 0.2 % offset yield strength, MPa
σ_{UTS} : Ultimate tensile strength, MPa
σ_{max} : Net section stress at maximum load

References

[1] J. R. Sims, Standards and codes to control hydrogen-induced cracking in pressure vessels and pipes for hydrogen gas storage and transport, P. Gangloff, B. Somerday (Eds.), *Gaseous Hydrogen Embrittlement of Materials in Energy Technologies,* Woodhead Publishing Limited, 1 (2012).

[2] G. R. Caskey Jr., *Hydrogen Compatibility Handbook for Stainless Steels No DP-1643*, Du Pont de Nemours (EI) and Co. Savannah River Lab, Aiken, SC (USA) (1983).

[3] H. Matsunaga, M. Yoshikawa, R. Kondo, J. Yamabe and S. Matsuoka, Slow strain rate tensile and fatigue properties of Cr–Mo and carbon steels in a 115 MPa hydrogen gas atmosphere, *Int. J. Hydrogen Energy*, 40 (2015) 5739-5748.

[4] *ASTM G142-98, Standard Test Method for Determination of Susceptibility of Metals to Embrittlement in Hydrogen Containing Environments at High Pressure*, *High Temperature, or Both,* ASTM International (2011).

[5] J. Yamabe, O. Takakuwa, H. Matsunaga, H. Itoga and S. Matsuoka, Hydrogen diffusivity and tensile-ductility loss of solution-treated austenitic stainless steels with external and internal hydrogen, *Int. J. Hydrogen Energy*, 42 (2017) 13289-13299.

[6] C. San Marchi, T. Michler, K. A. Nibur and B. P. Somerday, On the physical differences between tensile testing of type 304 and 316 austenitic stainless steels with internal hydrogen and in external hydrogen, *Int. J. Hydrogen Energy*, 35 (2010) 9736-9745.

[7] T. T. Nguyen, J. Park, S. H. Nahm, N. Tak and U. B. Baek, Ductility and fatigue properties of low nickel content type 316L austenitic stainless steel after gaseous thermal pre-charging with hydrogen, *Int. J. Hydrogen Energy*, 44 (2019) 28031-28043.

[8] T. T. Nguyen, H. M. Heo, J. Park, S. H. Nahm and U. B. Beak, Fracture properties and fatigue life assessment of API X70 pipeline steel under the effect of an environment containing hydrogen, *Journal of Mechanical Science and Technology*, 35 (2021) 1445-1455.

[9] L. Zhang, M. Imade, B. An, M. Wen, T. Iijima, S. Fukuyama and K. Yokogawa, Internal reversible hydrogen embrittlement of austenitic stainless steels based on type 316 at low temperatures, *ISIJ International*, 52 (2012) 240-246.

[10] H. Matsunaga, M. Yoshikawa, R. Kondo, J. Yamabe and S. Matsuoka, Slow strain rate tensile and fatigue properties of Cr–Mo and carbon steels in a 115 MPa hydrogen gas atmosphere, *Int. J. Hydrogen Energy*, 40 (2015) 5739-5748.

[11] L. Zhang, Z. Li, J. Zheng, Y. Zhao, P. Xu, X. Liu and X. Li, Influence of low temperature prestrain on hydrogen gas embrittlement of metastable austenitic stainless steels, *Int. J. Hydrogen Energy*, 38 (2013) 11181-11187.

[12] T. Michler and J. Naumann, Hydrogen environment embrittlement of austenitic stainless steels at low temperatures, *Int. J. Hydrogen Energy*, 33 (2008) 2111- 2122.

[13] S. J. Yoon, H. J. Lee, K. B. Yoon, Y. W. Ma and U. B. Baek, Hydrogen damage in 34CrMo4 pressure vessel steel with high tensile strength, *Journal of Mechanical Science and Technology*, 32 (2018) 637-646.

[14] T. T. Nguyen, H. M. Heo, J. Park, S. H. Nahm and U. B. Beak, Fracture properties and fatigue life assessment of API X70 pipeline steel under the effect of an environment containing hydrogen, *Journal of Mechanical Science and Technology*, 35 (2021) 1445-1455.

[15] T. T. Nguyen, H. M. Heo, J. Park, S. H. Nahm and U. B. Beak, Damage assessment and mechanical performance of Cr-Mo steel used in hydrogen storage vessels, *Engineering Failure Analysis*, 120 (2021) 105031.

[16] Z. Hua, X. Zhang, J. Zheng, C. Gu, T. Cui, Y. Zhao and W. Peng, Hydrogen-enhanced fatigue life analysis of Cr–Mo steel high-pressure vessels, *Int. J. Hydrogen Energy*, 42 (2017) 12005-12014.
[17] C. San Marchi, J. Yamabe, M. Schwarz, H. Matsunaga, S. Zickler, S. Matsuoka and H. Kobayashi, Global harmonization of fatigue life testing in gaseous hydrogen, *ASME 2018 Pressure Vessels and Piping Conference 2018* (2018) PVP2018-84267.
[18] T. Iijima, H. Enoki, J. Yamabe and B. An, Effect of high pressure gaseous hdyrogen on fatigue properties of SUS304 and SUS316 austenitic stainless steel, *ASME 2018 Pressure Vessels and Piping Conference 2018* (2018) PVP2018-84267.
[19] C. Zhou, Y. Hong, L. Zhang, B. An, J. Zheng and J., X. Chen, Abnormal effect of nitrogen on hydrogen gas embrittlement of austenitic stainless steels at low temperatures, *Int. J. Hydrogen Energy*, 41 (2016) 13777-13785.
[20] J. H. Holbrook, H. J. Cialone, E. W. Collings, E. J. Drauglis, P. M. Scott and M. E. Mayfield, *Control of Hydrogen Embrittlement of Metals by Chemical Inhibitors and Coatings*, Elsevier Inc. (2012) 129-153.
[21] R. Komoda, M. Kubota and J. Furtado, *Effect of Addition of Oxygen and Water Vapor on Fretting Fatigue Properties of an Austenitic Stainless Steel in Hydrogen*, Elsevier Ltd (2015) 16868-16877.
[22] H. Ez-Zaki, F. Christien, C. Bosch, L. Briottet, M. Bertin, O. Levasseur and A. Leriverain, Effect of hydrogen content in natural gas blend on the mechanical properties of a L485-MB low-alloyed steel, *ASME 2020 Pressure Vessels and Piping Conference 2020* (2020) PVP2020-21228.
[23] C. San Marchi, M. Schwarz and J. Ronevich, Effect of high-pressure hydrogen and water impurity on aluminum alloys, *Pressure Vessels and Piping Conference* (2020) PVP2020-21277.
[24] ANSI/CSA CHMC 1-2014, *Test Methods for Evaluating Material Compatibility in Compressed Hydrogen Applications-Metals*, CSA Gas Standards (2014).
[25] T. Ogata and Y. Ono, Influence of roughness of inner surface of simple mechanical testing method to evaluate influence of high-pressure hydrogen gas, *Pressure Vessels and Piping Conference 2019* (2019) PVP2019-93492.
[26] GTR Number 13-6-06, *Current Status of Round-Robin Tests for Hydrogen Material Compatibility*, Tianjin, China, June (2019).

Thanh Tuan Nguyen received his Ph.D. in Mechanical Engineering from Chung-Ang University, Korea in 2018. He is currently working as a post-doctoral fellow at the Korea Research Institute of Standard and Science. His research interests are failure analysis, high-temperature fracture mechanics and the effect of gaseous hydrogen environments on the mechanical properties of materials.

Jaeyeong Park received his Ph.D. in Material Science Engineering from Pohang University of Science and Technology, Korea in 2018. He is currently working as senior researcher at the Korea Research Institute of Standard and Science. His research interests are materials science and the mechanical behaviour of materials at high temperature, including anisotropic materials such as gas turbine blades.

Seung Hoon Nahm received his Ph.D. in Mechanical Engineering from Kyungpook National University, Korea in 1997. He is currently working as principal research scientist at the Korea Research Institute of Standard and Science. His research interests are the mechanical behaviour of materials at the micro and nano-scales, hydrogen embrittlement and mechanical behaviour of materials at high temperature.

Un Bong Baek received his Ph.D. in Mechanical Engineering from Kyungpook National University in 2001. He worked at Georgia Institute of Technology, U.S.A. as a post-doctoral fellow during 2002-2003. Dr. Baek is currently Director of the Centre for Energy and Material Metrology of KRISS (Korea Research Institute of Standards and Science). His research interest is in the mechanical behaviour of materials in high-pressure hydrogen environments.